# High-Frame-Rate Synthetic Aperture Ultrasound Imaging Using Mismatched Coded Excitation Waveform Engineering: A Feasibility Study

Bahman Lashkari, Kaicheng Zhang, and Andreas Mandelis

*Abstract*—**Mismatched coded excitation (CE) can be employed to increase the frame rate of synthetic aperture ultrasound imaging. The high autocorrelation and low cross correlation (CC) of transmitted signals enables the identification and separation of signal sources at the receiver. Thus, the method provides B-mode imaging with simultaneous transmission from several elements and capability of spatial decoding of the transmitted signals, which makes the imaging process equivalent to consecutive transmissions. Each transmission generates its own image and the combination of all the images results in an image with a high lateral resolution. In this paper, we introduce two different methods for generating multiple mismatched CEs with an identical frequency bandwidth and code length. Therefore, the proposed families of mismatched CEs are able to generate similar resolutions and signal-to-noise ratios. The application of these methods is demonstrated experimentally. Furthermore, several techniques are suggested that can be used to reduce the CC between the mismatched codes.**

*Index Terms*—**Chirp modulation, frequency modulation (FM), matched filters, pulse compression methods, synthetic aperture radar, synthetic aperture sonar.**

## Nomenclature

| | |
|---|---|
| AC | Autocorrelation of a signal. |
| AC/CC | Ratio of maximum AC of one code over its maximum cross correlation with other codes in decibels. |
| BW | Bandwidth (−6 dB). |
| CC | Cross correlation of a signal with another signal. |
| CE | Coded excitation. |
| CF | Center frequency. |
| DR | Dynamic range. |
| FC | Full cycle (carrier pattern for GC). |
| FG | Function generator. |
| FM | Frequency modulation (in this paper, we only considered linear frequency sweeps. The carrier signals are either sinusoidal or square shape, and thus, the more general term FM is used in most of the cases). |
| GC | Golay code. |
| GCF | Greatest common factor. |
| GSNR | Gain in signal-to-noise ratio. |
| HC | Half-cycle (carrier pattern for GC). |
| LFM | Linear FM (it implies both linear frequency sweep and sinusoidal wave carrier together). |
| MB-STMZ | Multibeam simultaneous transmit multizone. |
| MSR | Mainlobe-to-sidelobe ratio. |
| SNR | Signal-to-noise ratio. |
| TTF | Transducer transfer function. |
| US | Ultrasound or ultrasonic. |

Manuscript received January 13, 2016; accepted March 31, 2016. Date of publication April 14, 2016; date of current version June 1, 2016. This work was supported in part by the Canada Research Chairs Program, and in part by the Natural Sciences and Engineering Research Council of Canada (NSERC) Discovery Grants Program. The work of A. Mandelis was supported by the NSERC–Canadian Institutes of Health Research (CIHR) under a CHRP Grant.

The authors are with the Center for Advanced Diffusion-Wave Technologies, Department of Mechanical and Industrial Engineering, University of Toronto, Toronto, ON M5S 3G8, Canada (e-mail: bahman@mie.utoronto.ca; kc.zhang@mail.utoronto.ca; mandelis@mie.utoronto.ca).

Digital Object Identifier 10.1109/TUFFC.2016.2551705

## I. Introduction

MEDICAL ultrasound (US) system developers desire to enhance image quality, signal-to-noise ratio (SNR), and resolution, while at the same time, they must satisfy the real-time requirements for penetration depth and frame rate. Part of these features may be compromised with the level of system complexity. The advent of array transducers in US medical imaging in the late 1960s revolutionized the field; however, full utilization of the array capacity remained far behind, and that was due to the lack of required complex hardware. Enormous improvements have been accomplished since then and more are expected with advances in US front-end technology. This paper focuses on two of the most efficient and imaginative techniques devised to improve the frame rate and penetration depth of US imagers. Both methods are traced back to radar technology and were later adopted in US applications. Coded excitation (CE) has been utilized as a technique for increasing the SNR and penetration depth while preserving resolution [1]. On the other hand, synthetic aperture in addition to reducing the complexity and cost of the imaging system facilitates faster acquisition while making the best use of the steering capacity of the array [2]–[5]. The combination of these two methods is not a new idea [2], [6], [7], but the motivation is to benefit from the advantages of both. In this paper, we propose some novel methods that use CE more effectively to increase the SNR, depth penetration, and frame rate.

As mentioned before, using CE to enhance SNR and synthetic aperture in US transmission, reception, or both modes has been utilized by several investigators. An interesting related work is the synthetic transmit aperture using orthogonal Golay codes (GC) proposed by Chiao and Thomas [8], [9]. In their simulation, they used four transmitting elements in the form of two pairs of complementary codes. Employing a Hadamard matrix, they could decode the received signal at the expense of multiple transmissions. The use of long GCs or $m$-sequences, which generates very small correlation, has been suggested by Shen and Ebbini [10] and Kiymik *et al.* [11]. Very recently, the application of Hadamard-based delay-encoded transmission was also reported [12]. Misaridis and Jensen [2] proposed the use of two linear frequency modulation (LFM) waveforms with opposite slopes. Due to the mismatch of these codes, the number of transmissions for special decoding with the Hadamard matrix reduces to half, and at the same time, it can benefit from the higher SNR of frequency modulation (FM) [2]. Another approach is the use of a set of single frequencies or FM signals where each covers part of the transducer bandwidth (BW) and thus is uncorrelated [13], [14]. However, this method produces nonuniform resolution and SNR in the image. Another attempt for increasing the lateral resolution without sacrificing the frame rate was through a multibeam simultaneous transmit multizone (MB-STMZ) focusing method [15], [16]. This method was implemented by combining $M$ orthogonal GCs with $L$ orthogonal chirps to obtain $M$ scan lines each consisting of $L$ different focusing depths. The orthogonal GCs had a similar number of bits and were selected similar to [8]. The orthogonal chirps were generated by dividing the frequency bandwidth of the transducer. Examples were presented for the case where $M = L = 2$ [15], [16].

It should be added that very similar methods have been employed in other fields such as radar, sonar, and even wireless communications. These methods are readily applicable to biomedical US imaging and so are the methods presented in this paper. An overview of the relevant techniques in those fields is therefore valuable. An interesting method for sonar multibeam imaging is frequency hopping [17]. The BW is divided into a number of individual frequencies, and then, these frequencies are distributed distinctively using a frequency hopping code to produce uncorrelated waveforms. Using long mismatched pseudonoise sequences has also been suggested for multiple-transmission radar imaging [18]. The Hadamard encoding technique has been extensively employed in communication phase array antennas [19], [20].

The rationale of this work is to benefit from the high autocorrelation (AC) and low cross correlation (CC) of mismatched CEs. Therefore, in addition to SNR enhancement of CE, it also enables the simultaneous insonification from several elements of the ultrasonic transducer. Thus, each transmission generates its own image and the combination of all the images results in a high-resolution image. We more quantitatively elaborate on what is meant by high and low AC and CC: the AC/CC should be ideally in the same range of the signal SNR; otherwise, the CC of mismatched codes adds adverse effects to the image. The typical SNRs of US signals are 30–40 dB, and thus, an ideal AC/CC is in this range.

The contribution of this paper is in introducing two novel methods that can generate multiple mismatched codes with identical frequency and code length (duration). These methods are not only new in biomedical US, but they have never been employed in the related fields such as radar and sonar. The abovementioned methods are described in Sections II-A and II-B.

Section I explains the proposed methods and uses theory and simulations to demonstrate the CC and AC of mismatched codes. The proposed mismatched codes are based on FM chirps and GCs. The new waveform engineering methods can be used for any number of transmitting elements. Next, following the description of the generation of multiple mismatched codes, two sets of experiments are described that show the feasibility of the methods. Practical problems are discussed and some solutions are suggested.

## II. Design of Weakly Correlated (Mismatched) Waveforms

Here we start with a short review of two types of codes used in this paper: FM and GC. Both are capable of generating long codes. US experiments show that LFM generates the highest SNR [21]. On the other hand, the outstanding advantage of GC is the removal of sidelobes using two complementary codes [22].

An LFM signal can be defined as

$$r(t) = A\cos\left(\omega_c t + \frac{\pi B_{\mathrm{FM}}}{T_{\mathrm{FM}}}t^2\right)\mathrm{rect}\left(\frac{t}{T_{\mathrm{FM}}}\right) \tag{1}$$

where $T_{\mathrm{FM}}$ is the chirp duration, $B_{\mathrm{FM}}$ is the frequency BW of the chirp, $\omega_c$ is the central angular frequency of the chirp, and $A$ is the amplitude. These parameters can be optimized based on transducer transfer function (TTF) and other system considerations to provide the maximum SNR [23], [24]. In an ideal system, the response to (1) is its replica. For large time–BW products, the response of the matched filter is estimated as [25]

$$R(t) \approx A\frac{\sin(\mu T_{\mathrm{FM}}t/2)}{\mu t}\cos(\omega_c t)\mathrm{rect}\left(\frac{t}{2T_{\mathrm{FM}}}\right) \tag{2}$$

where $\mu = (2\pi B_{\mathrm{FM}}/T_{\mathrm{LFM}})$ is the slope and the peak value is $R_{\max} \approx A(T_{\mathrm{FM}}/2)$. For simplicity, we henceforth assume that the amplitude $A$ is unity. Equation (1) is the simplest and most popular FM chirp; however, alternatives to this have also been employed, for instance, nonlinear frequency sweeps [26] or square carrier waveforms [27], [28].

A GC is defined as a pair of $N$-bit length binary sequences, $A(k)(k = 0, 1, \ldots, N-1)$ and $B(k)$, which satisfies [22]

$$A(k) * A(-k) + B(k) * B(-k) = 2N\delta(k) \tag{3}$$

where $*$ represents convolution and $\delta(k)$ represents the Dirac delta function. Equation (3) shows that the signal enhancement is proportional to the length of the sequence, and ideally, no sidelobes are present. The frequency content of GCs can be manipulated by convolving the GC with a sinusoidal function. Using half-cycle (HC) sinusoids generates a very similar GC without sidelobes, as expected from a binary sequence. The benefit of employing FC carrier waves is discussed by Nowicki *et al.* [29]. However, it should be mentioned that the use of HC can be advantageous depending on the application [30]. The GC signal enhancement is proportional to $2N$, the length of the GC (or number of bits), regardless of carrier waveform.

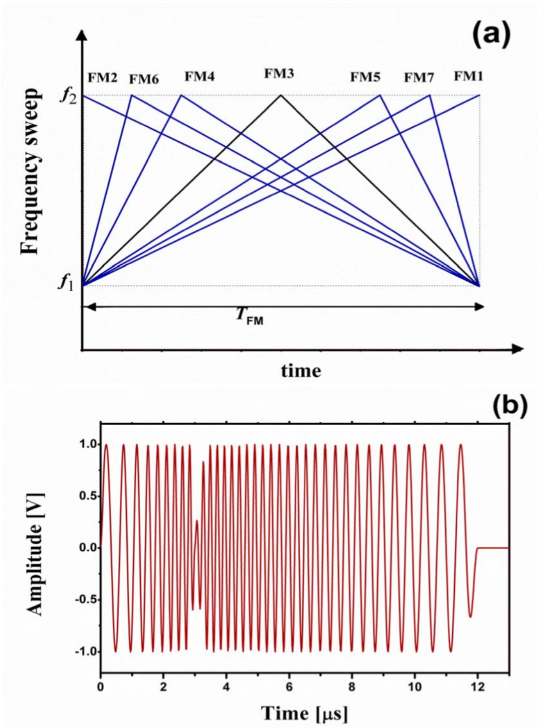


Fig. 1. (a) Frequency sweeps with an identical BW and duration, generating mismatched FM. (b) Waveform based on FM4: the frequency first sweeps up from 1.3 to 4.7 MHz and then sweeps down from 4.7 to 1.3 MHz with a different slope. Ten percent of tapering has been applied to each frequency sweep part.

### *A. Design of Mismatched Frequency-Modulation Waveforms*

Uncorrelated FM signals facilitate simultaneous transmission and decoding in receiver mode. This is like coloring or marking the transmission, so we can recognize the signal source. Mismatched FM waveforms can be designed using different parts of the BW or different duration times to change the FM slope. However, these methods generate nonuniform resolution and SNR in the image. The other option for only two FM signals is using the same BW and duration but reversing the frequency sweep with time. The limitation of this method is that only two FM signals can be generated [2].

Our approach is to produce multiple FM signals with an identical BW and duration, but with different slopes to mismatch the transmitted signals. The idea is to sweep the same frequency range at different rates. Fig. 1(a) shows seven frequency sweeps over time, all of which have the same time-BW product. FM1 and FM2 are the proposed chirps with opposite slopes [2]. FMs 3–7 divide the BW into two parts, a rising and a falling frequency sweep. Fig. 1(b) shows the waveform generated based on the frequency sweep patterns FM4 shown in Fig. 1(a). The desired mismatch is accomplished as long as the slopes of all sections are different. Obviously, this method has no limitation for making any arbitrary number of FMs. This is very important in facilitating the application of a large number of array elements and 3-D US imaging systems. A limitation to the number of independent chirps is the shortest time that the function generator (FG) instrument can allocate for each frequency as the sweep slope becomes steeper. However, with increasing chirp duration, it is always possible to reach the required frequency resolution.

A theoretical estimate for the CC of two LFM chirps with an identical BW and different slopes is developed in the Appendix. We use the results to estimate the CC of several FM signals consisting of one or two frequency sweep slopes. The CC of an FM (e.g., FM4) with other FMs, in the worst case equals the addition of their maximum CCs, which is when all the maxima coincide. Therefore, the CC of an FM with $N_i$ slopes ($N_i = 1$ or 2) with $n_s$ other FM signals, each consisting of $N_j$ slopes, is

$$\mathrm{CC}_{\max} \leq \frac{1}{2\sqrt{B_{\mathrm{FM}}}} \sum_{i=1}^{n_s} \sum_{m=1}^{N_i} \times \left\{ \sum_{n=1}^{N_j} \sqrt{\frac{T_{\mathrm{FM}i,m} T_{\mathrm{FM}j,n}}{\Delta T_{im,jn}}} + \frac{1}{2\sqrt{B_{\mathrm{FM}}}} \begin{cases} 0, & N_i = 1 \\ \sqrt{\frac{T_{\mathrm{FM}i,1} T_{\mathrm{FM}i,2}}{\Delta T_{i1,i2}}}, & N_i = 2 \end{cases} \right\}. \tag{4}$$

The second term shows the CC due to different slopes in the transmitted FM. Therefore, if the reference FM consists of only one frequency sweep, this term will be zero. $\Delta T$ is the difference between the duration of two frequency sweeps with the same BW and is defined by

$$\Delta T_{im,jn} = |\mathrm{sign}(\mu_{jn}) T_{\mathrm{FM}i,m} - \mathrm{sign}(\mu_{im}) T_{\mathrm{FM}j,n}| \tag{5}$$

where $\mu$ is the slope of the frequency sweep (Appendix). Here, the direction of slopes is important (upchirp versus downchirp). Therefore

$$\frac{\mathrm{CC}_{\max}}{\mathrm{AC}_{\max}} \leq \frac{1}{T_{\mathrm{FM}}\sqrt{B_{\mathrm{FM}}}} \sum_{i=1}^{n_s} \sum_{m=1}^{N_i} \times \left\{ \sum_{n=1}^{N_j} \sqrt{\frac{T_{\mathrm{FM}i,m} T_{\mathrm{FM}j,n}}{\Delta T_{im,jn}}} + \frac{1}{T_{\mathrm{FM}}\sqrt{B_{\mathrm{FM}}}} \begin{cases} 0, & N_i = 1 \\ \sqrt{\frac{T_{\mathrm{FM}i,1} T_{\mathrm{FM}i,2}}{\Delta T_{i1,i2}}}, & N_i = 2 \end{cases} \right\}. \tag{6}$$

The proposed method can be illustrated by means of a simulation of some mismatched FM signals. Fig. 2 shows a set of simulated CC signals among some FM chirps. The simulations were performed with the LabView platform (National Instruments, Austin, TX, USA). All FM signals have the same frequency range between 1.3 and 4.7 MHz. The chirp durations are 23.47 and 187.7 $\mu$s for Fig. 2(a) and (b), respectively. Fig. 2(a) and (b) shows the AC of FM4 and its CC with FM2, FM3, and FM5. It can be seen that there is a minor CC among the various FM signals, which decreases with increasing chirp duration. The simulation of these FMs has been performed for a wide range of chirp durations, considering both sinusoidal and square carrier waves. In the simulations, the effect of TTF was also considered. The TTF was modeled with a bell shape (cosine squared) function [23]. In the simulations, a transducer with a center frequency (CF) of 3 MHz and a fractional BW of 70% was assumed. The ratio of the maximum CC of FM4 with other waveforms to the peak of FM4 AC (CC/AC) is shown in Fig. 2(c). The chirp duration starts with 23.47 $\mu$s to a maximum of 6.007 ms. The chirp duration defines the frequency sweep slope and is arbitrary. Fig. 2(c) shows the decrease of CC/AC for four cases: sinusoidal carrier and square carrier without and with consideration of the TTF effect. The conclusion is that regardless of the carrier signal and filtering, the CC/AC decreases with increasing duration. Using (6) and the FM signals used in the example, the theoretical upper limit of CC/AC can be calculated. This theoretical upper limit is also shown in Fig. 2(c). It can be seen that by increasing the total duration time $T_{\mathrm{FM}}$, the $\Delta T$s between frequency sweep slopes are increased proportionally. Therefore, the CC/ACs decrease. As a result

$$\frac{\mathrm{CC}_{\max}}{\mathrm{AC}_{\max}} \leq \frac{8.45}{\sqrt{T_{\mathrm{FM}} B_{\mathrm{FM}}}} = \frac{0.0046}{\sqrt{T_{\mathrm{FM}}}}. \tag{6a}$$

### *B. Combined Golay Code and Frequency Modulation*

The choice of the carrier waveform for a GC has been discussed before [29]. Typical carrier waveforms are either HC or full-cycle (FC) sinusoidal or square waves. We show here that it is possible to use a complete chirp as the carrier signal of a GC. In other words, the chirps can be coded to generate a new CE. The pulse compression signal of such a CE can be calculated in a manner very similar to a conventional GC. The pulse compression of each part is calculated with its corresponding code and the two matched filter signals are added to yield the final pulse compressed signal. This operation may seem useless in the sense that the new CE will not increase the SNR or gain in SNR (GSNR); in fact, it will lose the main advantage of GC, which is being sidelobe free. The SNR and GSNR are similar to an FM signal with the same frequency range and the total duration of the signal as the time and BW will be identical. However, the goal pursued here is to generate mismatched CEs and the combined GC FM is able to do that.

To present it in a more rigorous way, we can describe the continuous GC signal as the convolution of an HC cosine and a train of spikes with multipliers equal to the GC coefficients. The duration of the half cycle cosine and intervals between spikes ($\delta$: Dirac delta function) are equal to $T/N$. The continuous time equivalent of GCs in (3) will be

$$\begin{aligned} g_A(t) &= \sum_{i=0}^{N-1}\left(A_{\mathrm{gc}}(i)\delta\left(t-\frac{iT}{N}\right)\right) \\ &\quad * \left[\cos\left(\frac{\pi N t}{T}\right)\mathrm{rect}\left(\frac{Nt}{T}\right)\right] \\ g_B(t) &= \sum_{i=0}^{N-1}\left(B_{\mathrm{gc}}(i)\delta\left(t-\frac{iT}{N}\right)\right) \\ &\quad * \left[\cos\left(\frac{\pi N t}{T}\right)\mathrm{rect}\left(\frac{Nt}{T}\right)\right]. \end{aligned} \tag{7}$$

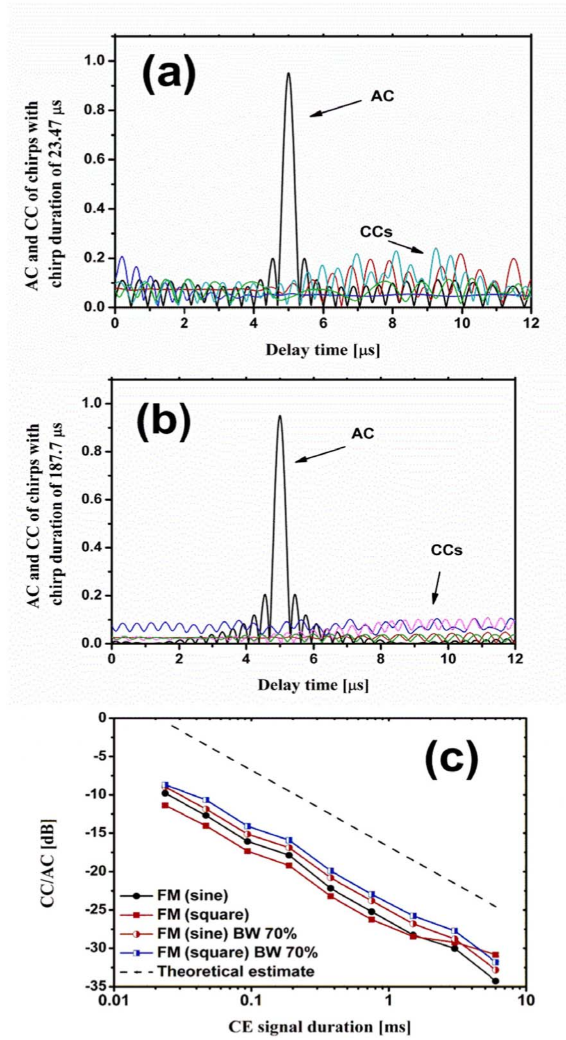


Fig. 2. AC of FM4 and CC of FM4 with FM2, FM3, and FM5 for chirp durations. (a) 23.47 $\mu$s. (b) 187.7 $\mu$s (simulation). (c) Decrease in the maximum CC of FM4 with FM1, and FM3 to FM5 to FM4 AC peak (CC/AC) for chirp durations from 23.47 $\mu$s to 6.007 ms. The theoretical upper limit of CC/AC is shown as a dashed straight line. The simulations were performed for different cases of sinusoidal and square waveforms, with and without the transducer effect (70%).

Here, $A_{\mathrm{gc}}$ and $B_{\mathrm{gc}}$ are complementary $N$-bit GCs and $T$ is the total duration of each signal ($g_A$ or $g_B$). The matched filter sum of GC is

$$R_{AB\cos}(t) = g_A(t) * g_A(-t) + g_B(t) * g_B(-t). \tag{8}$$

Using the associative property of convolution, $R_{\mathrm{ABcos}}$ can be calculated

$$\begin{aligned} &R_{AB\cos}(t) \\ &= \left[\sum_{i=0}^{N-1}\left(A_{\mathrm{gc}}(i)\delta\left(t-\frac{iT}{N}\right)\right) * \sum_{i=0}^{N-1}\left(A_{\mathrm{gc}}(i)\delta\left(\frac{iT}{N}-t\right)\right)\right. \\ &\quad \left. + \sum_{i=0}^{N-1}\left(B_{\mathrm{gc}}(i)\delta\left(t-\frac{iT}{N}\right)\right) * \sum_{i=0}^{N-1}\left(B_{\mathrm{gc}}(i)\delta\left(\frac{iT}{N}-t\right)\right)\right] \\ &\quad * \left[\left[\cos\left(\frac{\pi N t}{T}\right)\mathrm{rect}\left(\frac{Nt}{T}\right)\right] * \left[\cos\left(\frac{\pi N t}{T}\right)\mathrm{rect}\left(\frac{Nt}{T}\right)\right]\right]. \end{aligned} \tag{9}$$

Using the definition of GC, we obtain

$$\sum_{i=0}^{N-1}\left(A_{\mathrm{gc}}(i)\delta\left(t-\frac{iT}{N}\right)\right)*\sum_{i=0}^{N-1}\left(A_{\mathrm{gc}}(i)\delta\left(\frac{iT}{N}-t\right)\right)$$
$$+\sum_{i=0}^{N-1}\left(B_{\mathrm{gc}}(i)\delta\left(t-\frac{iT}{N}\right)\right)*\sum_{i=0}^{N-1}\left(B_{\mathrm{gc}}(i)\delta\left(\frac{iT}{N}-t\right)\right)$$
$$=2N\delta(t). \tag{10}$$

By direct integration, it can be shown that

$$\left[\cos\left(\frac{\pi Nt}{T}\right)\mathrm{rect}\left(\frac{Nt}{T}\right)\right]*\left[\cos\left(\frac{\pi Nt}{T}\right)\mathrm{rect}\left(\frac{Nt}{T}\right)\right]$$
$$=\left[\frac{1}{2}\left(\frac{T}{N}-|t|\right)\cos\left(\frac{\pi Nt}{T}\right)-\frac{T}{2\pi N}\sin\left(\frac{\pi N|t|}{T}\right)\right]$$
$$\times\mathrm{rect}\left(\frac{Nt}{2T}\right). \tag{11}$$

Therefore

$$R_{AB\cos}(t)=2N\delta(t)*\left[\frac{1}{2}\left(\frac{T}{N}-|t|\right)\cos\left(\frac{\pi Nt}{T}\right)\right.$$
$$\left.-\frac{T}{2\pi N}\sin\left(\frac{\pi N|t|}{T}\right)\right]\mathrm{rect}\left(\frac{Nt}{2T}\right)$$
$$=\left[(T-N|t|)\cos\left(\frac{\pi Nt}{T}\right)-\frac{T}{\pi}\sin\left(\frac{\pi N|t|}{T}\right)\right]\mathrm{rect}\left(\frac{Nt}{2T}\right). \tag{12}$$

Similarly, the convolution of GC and LFM chirp can be calculated as

$$e_A(t)=\sum_{i=0}^{N-1}(A_{\mathrm{gc}}(i)\delta(t-iT_{\mathrm{FM}}))$$
$$*\left[\cos\left(\omega_c t+\frac{\pi B_{\mathrm{FM}}}{T_{\mathrm{FM}}}t^2\right)\mathrm{rect}\left(\frac{t}{T_{\mathrm{FM}}}\right)\right] \tag{13a}$$
$$e_B(t)=\sum_{i=0}^{N-1}(B_{\mathrm{gc}}(i)\delta(t-iT_{\mathrm{FM}}))$$
$$*\left[\cos\left(\omega_c t+\frac{\pi B_{\mathrm{FM}}}{T_{\mathrm{FM}}}t^2\right)\mathrm{rect}\left(\frac{t}{T_{\mathrm{FM}}}\right)\right] \tag{13b}$$

where $T_{\mathrm{FM}}=T/N$. Similar to HC sequential codes, the AC result of combined GC–FM is

$$R_{AB\mathrm{chirp}}(t)=e_A(t)*e_A(-t)+e_B(t)*e_B(-t). \tag{14}$$

Again using the associative property of convolution and implementing the AC of a chirp by means of (2) and (10)

$$R_{AB\mathrm{chirp}}(t)=2N\frac{\sin(\mu T_{\mathrm{FM}}t/2)}{\mu t}\cos(\omega_c t)\mathrm{rect}\left(\frac{t}{2T_{\mathrm{FM}}}\right). \tag{15}$$

The proposed method can be explained by means of an example. Fig. 3(a) and (b) shows a 4-bit HC GC and a chirp, respectively. Both have the same duration of 12 $\mu$s. The complementary part of the GC is transmitted after detecting the response to the first part, for instance, after 150 $\mu$s [Fig. 3(a)]. The GC is $[1,-1,1,1]$ and its complementary code is $[-1,1,1,1]$. Similarly, the same chirp is transmitted again after enough delay to detect the complete response to the first code, that is, after 150 $\mu$s. A chirp can be considered as a 1-bit GC with complementary parts of [1] and [1]. If the duration of the signal is fixed at 12 $\mu$s [same as the FM signal in Fig. 3(b)], a chirp introduced as the carrier waveform of GC results in the combined GC and FM shown in Fig. 3(c). Hence, the duration of each part of the 4-bit GC is 3 $\mu$s. The complementary code is produced similarly. Here we can comment on the differences between the combination of GC and chirp proposed here and MB-STMZ [15], [16]. The latter is based on using orthogonal GCs, whereas here, GCs do not need to be orthogonal but should consist of different numbers of bits. MB-STMZ is based on chirps with different frequency ranges, whereas the proposed method uses chirps with an identical BW but different durations; $T/N_1, T/N_2, \ldots,$ where $T$ is the duration of each complementary part of the excitation signal and $N_1, N_2, \ldots$ are numbers of bits of the employed GCs.

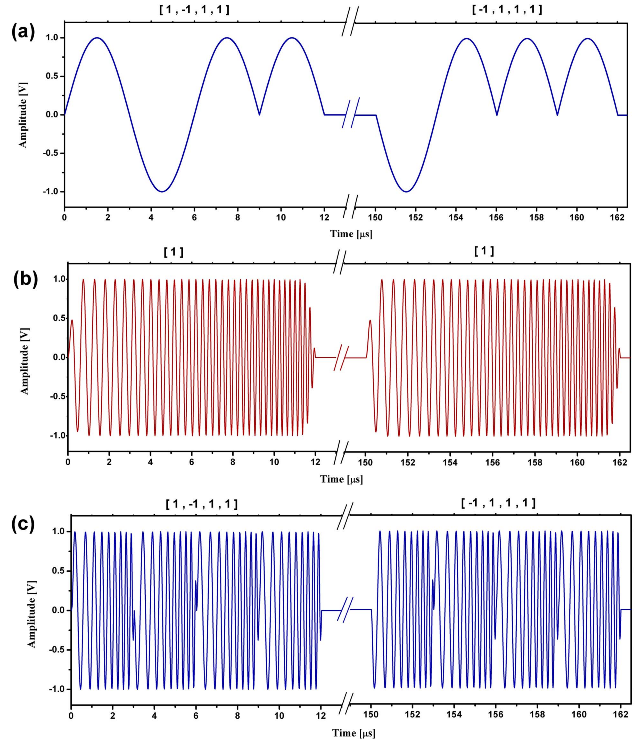


Fig. 3. (a) A 4-bit half cycle (HC) GC and its complementary code transmitted after 150 $\mu$s. (b) A FM chirp of 12 $\mu$s duration and frequency range 1.6-4.3 MHz, transmitted again after 150 $\mu$s. (c) A 4bit GC with carrier waveform of a 3 $\mu$s FM and similar frequency range as (b). After 150 $\mu$s, the complementary combined GCFM is transmitted.

Now we can consider the matched filtering of codes introduced in Fig. 3. Matched filtering of each part of the combined GC–FM generates a mainlobe and several sidelobes very similar to that of each part of a conventional GC. Nevertheless, the sidelobes cancel each other out when the ACs of the complementary parts are added together. Fig. 4(a) compares the matched filtering of GC and combined GC–FM introduced in Fig. 3(a) and (c), respectively. The final pulse compression of the combined GC–FM is shown in Fig. 4(b) and it is compared with the pulse compression of a chirp [Fig. 3(b)]. It should be added that the duration of the combined GC–FM assumed in this example was relatively short. Each frequency sweep was produced with only a few cycles. As the chirps in

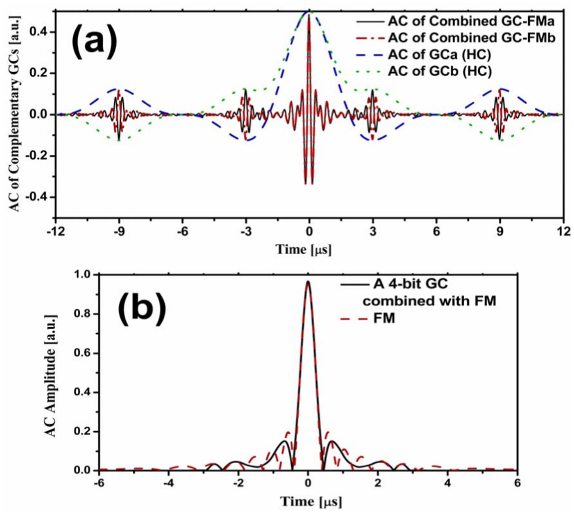


Fig. 4. (a) Pulse compression of complementary conventional 4-b GC [Fig. 3(a)] and a combined GC–FM [Fig. 3(c)]. The AC of each part of the combined GC–FM generated sidelobes that are out of phase with the other AC; similar to the conventional GC, sidelobes cancel each other out. (b) Results of pulse compression for FM in Fig. 3(b) and combined GC–FM in Fig. 3(c). Here, the complementary pulse compressions are added together and then enveloped (simulation).

the combined GC–FM become longer, the shapes of their pulse compression (and particularly the sidelobes) will resemble more a conventional FM. The main result is that the combined GC–FM generated a signal enhancement and resolution identical to a conventional chirp, while they are mismatched among themselves. Therefore, the proposed method can effectively generate multiple mismatched CEs. Other combined GC–FMs can be produced in the same manner, by employing GCs with 2, 8, 10, 16, 26 bits, and so on. This can be readily confirmed by considering two sets of GCs ($A_{\mathrm{gc}}(k)$, $B_{\mathrm{gc}}(k)$) and ($C_{\mathrm{gc}}(k)$, $D_{\mathrm{gc}}(k)$) with $N_1$ and $N_2$ being the number of bits. It is assumed that these codes have been convoluted with two chirps with the same BW and durations $T/N_1$ and $T/N_2$, respectively. The maximum amplitude of the matched filters is

$$R_{AB\mathrm{chirp}}(t)|_{\max} = 2N_1\left[\frac{1}{\mu_1 t}\sin\left(\frac{\mu_1 T t}{2N_1}\right)\cos(\omega_c t)\mathrm{rect}\left(\frac{N_1 t}{2T}\right)\right]_{t=0} = T. \tag{16}$$

Similarly, we obtain $R_{CD\mathrm{chirp}}(t)|_{\max} = T$.

The mismatched filter can be calculated as

$$R_{\mathrm{mismatch}\ AB-CD}(t) = e_C(t) * e_A(-t) + e_D(t) * e_B(-t). \tag{17}$$

To calculate the terms in (17), we must consider that coefficients of the selected GCs are unrelated. The only restriction is the different number of bits: $N_1$ and $N_2$. In the worst case, the correlations of the GC coefficients do not cancel each other out but are summed up. Therefore, the maximum values of the CCs may occur when the maximum number of $\delta$-functions coincides. The spikes of the first and second GCs happen at $T/N_1$ and $T/N_2$ intervals, respectively. Therefore, the maximum possible number of coincident spikes is GCF($N_1$, $N_2$) with intervals T/GCF($N_1$, $N_2$), where GCF($N_1$, $N_2$) is the greatest common factor between $N_1$ and $N_2$. As a result, the following relations are obtained:

$$\left\{\sum_{i=0}^{N_2-1}\left(C_{\mathrm{gc}}(i)\delta\left(t-\frac{iT}{N_2}\right)\right) * \sum_{i=0}^{N_1-1}\left(A_{\mathrm{gc}}(i)\delta\left(\frac{iT}{N_1}-t\right)\right)\right\}_{\max} \leq \mathrm{GCF}(N_1, N_2)\delta(t) \tag{18a}$$

$$\left\{\sum_{i=0}^{N_2-1}\left(D_{\mathrm{gc}}(i)\delta\left(t-\frac{iT}{N_2}\right)\right) * \sum_{i=0}^{N_1-1}\left(B_{\mathrm{gc}}(i)\delta\left(\frac{iT}{N_1}-t\right)\right)\right\}_{\max} \leq \mathrm{GCF}(N_1, N_2)\delta(t). \tag{18b}$$

It should be added that the maxima predicted in (18a) and (18b) are possible cases; however, it is also possible to reduce the CC by a careful choice of GC sets. For instance, one can readily calculate the maximum of the summation of the CCs between the 2- and 4-bit GCs in Table I, that is, 2GCF(2, 4) = 4. However, by performing a very simple operation, such as reversing the order or changing the sign of one part of one of the complementary codes, the CC summation peak reduces to 2.

The CC of two chirps $r_1(t)$ and $r_2(t)$ (to be combined with GCs with $N_1$ and $N_2$ bits) is

$$\begin{aligned} r_1(t) * r_2(-t) &= \left[\cos\left(\omega_c t + \frac{\pi N_1 B_{\mathrm{FM}}}{T}t^2\right)\mathrm{rect}\left(\frac{N_1 t}{T}\right)\right] \\ &\quad * \left[\cos\left(\omega_c t - \frac{\pi N_2 B_{\mathrm{FM}}}{T}t^2\right)\mathrm{rect}\left(\frac{N_2 t}{T}\right)\right]. \end{aligned} \tag{19}$$

Using (A-13) yields

$$|r_1(t) * r_2(-t)|_{\max} \approx \frac{1.2T}{2\sqrt{N_1 N_2 B_{\mathrm{FM}}\Delta T}}. \tag{20}$$

Using the associative property of convolution and substituting (18a), (18b), and (20) into (17), it can be shown that

$$R_{\mathrm{mismatch}\ AB-CD}(t)|_{\max} \leq \frac{1.2T}{\sqrt{N_1 N_2 B_{\mathrm{FM}}\Delta T}.}\mathrm{GCF}(N_1, N_2). \tag{21}$$

From (15), it can be concluded that

$$\frac{\mathrm{CC}_{\max}}{\mathrm{AC}_{\max}} = \frac{R_{\mathrm{mismatch}\ AB-CD}(t)|_{\max}}{R_{AB\mathrm{chirp}}(t)|_{\max}} \leq \frac{1.2\mathrm{GCF}(N_1, N_2)}{\sqrt{N_1 N_2 B_{\mathrm{FM}}\Delta T}} \tag{22}$$

where $\Delta T$ can be described based on total signal duration and GC bits

$$N_1 N_2 \Delta T = |\mathrm{sign}(\mu_1)N_2 - \mathrm{sign}(\mu_2)N_1| \cdot T. \tag{23}$$

Therefore, the CC/AC of a combined GC–FM with $N_i$ bits with $n$ other combined GC–FMs each with $N_j$ bits is

$$\frac{\mathrm{CC}_{\max}}{\mathrm{AC}_{\max}} \leq \sum_{j=1}^{n}\frac{1.2\mathrm{GCF}(N_i, N_j)}{\sqrt{N_i N_j B_{\mathrm{FM}}\Delta T}}. \tag{24}$$

Using a simulation, the variation of the CC/AC ratio with changing code duration among some combined codes was investigated. The AC of a combined code, generated by a 10-bit GC and the upchirp FM, as well as its CC among

TABLE I
GC USED FOR COMBINED GC–FM SIGNALS

| GCs | Complementary elements of GC |
|---|---|
| 1-bit | [1] & [1] |
| 2-bit | [1,1]&[1,-1] |
| 4-bit | [1,1,-1,1]&[1,1,1,-1] |
| 8-bit | [1,1,1,-1,1,-1,1,1] & [1,1,1,-1, -1,1,-1,-1] |
| 10-bit | [1,1,-1,1,-1,1,-1,-1,1,1] & [1,1,-1,1,1,1,1,1,-1,-1] |
| 16-bit | [1,1,1,-1,1,1,-1,1,1,1,1,-1, -1,-1,1,-1] & [1,1,1,-1,1,1,-1,1,-1,-1,-1,1,1,1,-1,1] |

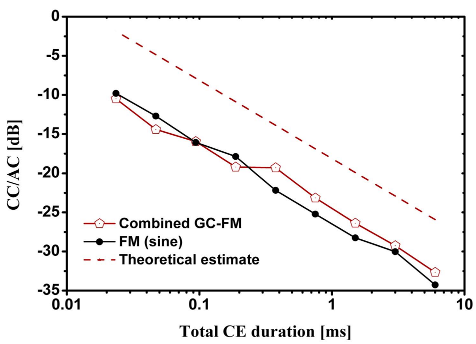


Fig. 5. Maximum CC to the peak AC ratio (CC/AC) of FM signals and combined GC–FM signals showing its decrease with increasing code duration (simulation). The dashed line is the theoretical upper limit of CC/AC for the combined GC–FM signals.

five other codes was calculated. The other codes were produced from 1-, 2-, 4-, 8-, and 16-bit GCs and the upchirp FM. The employed GCs are shown in Table I. Fig. 5 shows the decrease in CC/AC ratio with increasing code duration. Fig. 5 shows similar trends for an FM signal with the same duration as both complementary combined GC–FM codes. From (24) and the combined GC–FM signals used in the example, the theoretical upper limit of CC/AC can be calculated and is also shown in Fig. 5. The result of the calculation is

$$\frac{\mathrm{CC}_{\max}}{\mathrm{AC}_{\max}} \leq \frac{5.11}{\sqrt{\mathrm{TB}_{\mathrm{FM}}}} = \frac{0.0039}{\sqrt{2T}} \tag{24a}$$

where $2T$ is the total duration of the excitation with both complementary parts. The presented FM and combined GC–FM signals in Section II generate a main lobe width and mainlobe-to-sidelobe ratio (MSR) similar to an LFM with the same BW. If the MSRs are not large enough, proper filtering can help reduce the sidelobes [21]. Were the MSR generated by each code different, each code would require its own filter parameters which would have significantly increased the complexity of the system. Therefore, it is an important advantage to produce a similar MSR among all transmitted codes.

## III. Cross-Correlation Reduction Between Mismatched Signals

The SNR of a US signal should be high enough to generate a proper quality image. Thus, the CCs among simultaneously transmitted mismatched signals should be in the same range to maintain the quality of the image (ideally 30–40 dB and at least 14 dB). Nonzero CCs appear like artifacts in the image and consecutive measurements and averaging will not reduce them. The obvious solution is to increase the signal duration, but this may not be possible due to practical issues such as limited memory of the acquisition card and small depth of field [7]. Rather than increasing the signal duration, several techniques can be applied to reduce the CC between proposed mismatched signals. All these proposed methods require consecutive measurements that decrease the frame rate. In addition, they increase the complexity of the imaging system. Therefore, a compromise between all the conflicting requirements lies in the following approaches. Assuming several mismatched codes are transmitted simultaneously, we have the following techniques.

1) *Technique 1:* The starting phase of some of the signals can change irregularly in consecutive transmissions.
2) *Technique 2:* Similarly, the starting point of some transmitted signals can shift irregularly in consecutive transmissions.
3) *Technique 3:* Various combinations of the array elements can be employed for the transmission, and thus, in each consecutive transmission, the locations of the adjacent signal sources shift.
4) *Technique 4:* The transmitted CE can switch between the elements or change in each transmission.

The idea behind all these techniques is to either move or change the CCs in each consecutive insonification. Therefore, the artifacts move or change with each measurement and reduce when averaged over several measurements. The authentic signals (ACs) are not affected by these techniques as long as the pulse compressions are calculated with the corresponding transmissions. These techniques have some similarity to the techniques suggested for reducing speckle artifacts in B-mode US imaging [31]. A series of simplified simulations is presented here to demonstrate how this approach works. In the simulations, the mismatched codes of FM chirp signals introduced in Section II-A were used; however, the techniques can be applied to other CEs as well.

In one simulation, the AC of FM1 and its CC with FM4 were determined. The sweep patterns of FM1 and FM4 are shown in Fig. 1(a). FM1 is a normal upchirp and FM4 is an upchirp in one third of the duration and a downchirp in the remaining two thirds of the duration. The duration of the chirps was set to 12 $\mu$s and the BW was 1.6–4.3 MHz. The peak AC to maximum CC ratio (AC/CC) was 9.5 dB. The same simulation was repeated five times while the starting phase of the FM4 was changed in each consecutive transmission. The starting phases were 0°, 34°, −45°, 76°, and 6°. The coherently averaged CC between FM1 and FM4 was diminished, and hence, the AC/CC increased to 25 dB. Coherent averaging indicates that the phases of the individual signals affect the averaged value. The detailed description can be found elsewhere [28], [32]. Fig. 6(a) shows the AC and the first CC as well as the averaged CC.

In the next simulation, the AC of FM1 and the CC of FM1 and FM4 were considered again. The starting time of FM4

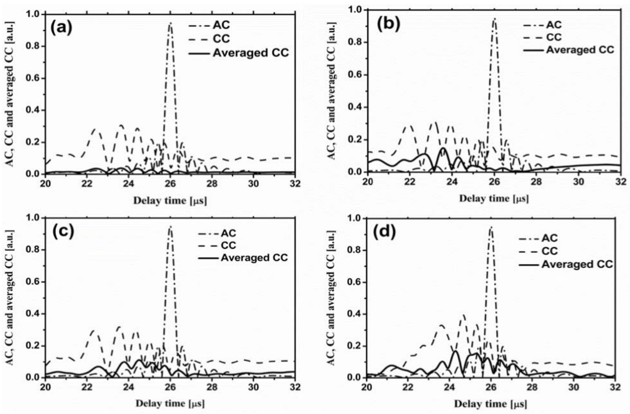


Fig. 6. (a) AC of FM1 and CC of FM1 and FM4, and the averaged CC when the phase of FM4 changes with each transmission. (b) AC of FM1, the CC of FM1 and FM4, and the averaged CC when the starting time of FM4 changes with each transmission (the time change is less than 1 $\mu$s). (c) AC of FM1 and CC of FM1 and FM4, and the averaged CC when the element transmitted FM4 switches in each transmission. (d) AC of FM1 and CC of FM1 with other chirps with the maximum value and averaged CC when the chirp changes in each transmission.

changed in each consecutive transmission. In the simulation, the starting times of the transmissions were 0, 0.3, 0.5, 0.7, and 0.8 $\mu$s. The signal CCs were calculated and coherently averaged. Fig. 6(b) shows the first and averaged CCs as well as the AC where the AC/CC ratio has been increased from 9.5 to 16 dB.

Another simulation demonstrates the effect of changing the adjacent transmitted elements. Only the effect of changing the location of adjacent concurrent transmitted signals in the delay time of the received signal is considered here. Consequently, the simulations are very similar to the results presented in Fig. 6(b). To obtain a realistic estimate of the delay time change with element change, we considered a phased array transducer with a pitch size of 0.254 mm and a sole scatterer located 20 mm in front of the element that transmitted FM1. If the adjacent transmitting element was the third transmitting element and it transmitted FM4, the CC of FM1 and FM4 and the AC of FM1 are shown in Fig. 6(c). Now, if the transmission is repeated from the first element while the element of the concurrent transmission is located at the 6th, 9th, 12th, and 15th rows. The corresponding received signal will be delayed by 0.38, 0.085, 0.15, and 0.234 $\mu$s, respectively. Fig. 6(c) shows the coherently averaged CC between FM1 and FM4 with the abovementioned delays. This simulation shows that the averaging process following permuting the adjacent transmitter element increased the AC/CC ratio from 9.5 to 18.6 dB.

A final simulation was based on changing the concurrent transmitting CEs. FM1 was considered as a fixed CE when the concurrent CE changes from FM2 to FM6 [Fig. 1(a)]. Fig. 6(d) shows the AC of FM1 and its CC with one of the CEs (the one that generates the maximum CC value). Fig. 6 also shows the average of five CCs. The averaging process increased the AC/CC ratio from 7.6 to 15 dB.

We conclude that all these techniques are beneficial in reducing the CCs and hence the artifacts. The complexity these techniques add to the system is an essential factor in choosing

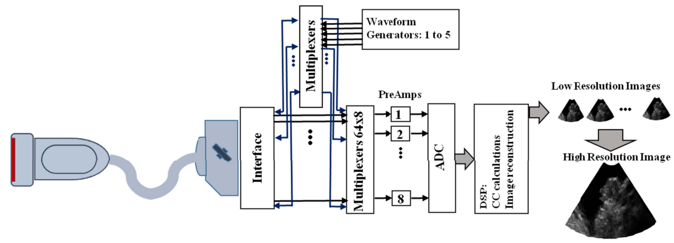


Fig. 7. Schematic of the experimental US imager.

one or a combination of them. It should be mentioned that except for the last technique, switching the CE in each transmission, the other techniques (techniques 1–3) have very similar effects, and therefore, there is no need to employ all of them. Technique 4 changes the CC shape by changing the transmitted CE in each insonification, but the other three methods mainly shift the CC in consecutive transmissions. As mentioned, the use of these techniques is conflicting with the goal of increasing the frame rate. The idea is to compensate for the extra time required for collecting multiple sets of data and performing averaging with the simultaneous transmissions, thereby reducing the total duration. This results in simultaneously increasing the frame rate and image quality. Furthermore, this scheme has a positive effect in reducing motion artifacts. To make this point clear, we can consider 64 elements planned to be used one at a time for transmission in conventional US imaging. Replacing this schedule with eight simultaneous transmissions, the total duration will decrease by a factor of eight, and thus, the presented method allows averaging up to eight times more; however, it is still affected by motion artifacts similar to the conventional method. Or alternatively, one can use less than eight times averaging and thus decrease the acquisition time and motion artifacts.

## IV. Instrumentation and System Implementation

The experimental setup was originally designed for solely receiving phased array transducers [33] (Fig. 7). The acquisition system was designed and programmed to collect 64-element transducer signals via eight subarray sections. The synchronization of different devices and the data acquisition procedure was controlled by a home-made LabView program (National Instruments, Austin, TX, USA). An eight-channel analog-to-digital converter (PXI-5105, NI) was employed to acquire the received waveforms, eight at a time. A virtual switch was programmed to control four multiplexer boards PXI-2593 (NI), which directed the subarray elements to eight preamps (HD28082, 40 dB, HD Communications Corporation) and reached the digitizer board. This arrangement facilitated an automated sweep through the subarrays and therefore provided a fairly fast acquisition rate with minimum complexity. The LabView program was employed to collect the response waveform of each subarray section and average the waveforms coherently [28]. Afterward, the CC signals of all channels with the transmitted signals were calculated. As discussed earlier, no extra filtering was applied to the received signals or during postprocessing. From the CC of all receiving elements with each of the designated CEs, an image was generated [5]. Subsequently, all such images were combined to generate

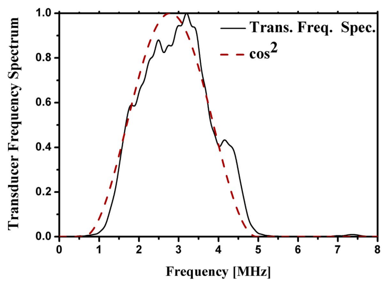


Fig. 8. TTF compared with a cosine squared function reveals the fractional BW of the transducer.

the final high-resolution image. The patterns for transmitting signals and active elements are discussed later.

The employed transducer was a 64-element phased array SA4-2/24 (Ultrasonix, BC, Canada). The BW of the transducer was 2–4 MHz with a 0.254-mm element pitch and a 12-mm elevation aperture. The TTF of the transducer elements was acquired by transmitting an LFM with a frequency sweep between 200 kHz and 8 MHz and detecting the reflection signal from a polished metal. The obtained TTF (Fig. 8) is very close to the assumed cosine squared function that was suggested for chirp optimization [27]. By matching the full-width at half maximum (FWHM) of the cosine squared and the acquired TTF, the fractional BW of the transducer was estimated to be 78%. This specifies the optimal BW for FMs to be in the 1.6–4.3-MHz range.

## V. Experimental Results

One of the limitations of employing CE techniques for medical US imaging is the short depth of field, which limits the transmit signal duration [7]. Curbing the maximum length of the transmitted code limits the maximum achievable SNR enhancement and the efficiency of the matched filter. To tackle this problem as well as reduce the complexity of the system, in Section V-A, we examine the use of long codes without switching the transmitter elements to become receivers. This simple configuration was used to demonstrate the feasibility of the method. However, the presented method has its challenges due the large crosstalk between the transducer elements. It is also possible to use short codes and average over more successive transmissions: this approach facilitates the use of techniques introduced in Section III for reducing the CC among simultaneously transmitting codes. The latter approach was examined in Section V-B.

### *A. Feasibility Test With Five Transmitting Elements*

For the first feasibility test, five elements out of a 64-element array were disconnected from the multiplexer and were connected to the FG devices. The transmit elements were #6, 19, 32, 45, and 58, which were used to insonify the field. The last four elements were emulated by two dual-channel analog waveform generators (33500B, Agilent Technologies Inc., Santa Clara, CA, USA). These waveform generators are capable of transmitting arbitrary waveforms and are therefore suitable for the complex waveforms proposed in Section II. Element 6 was imitated by an FG board PXI-5442 (NI),

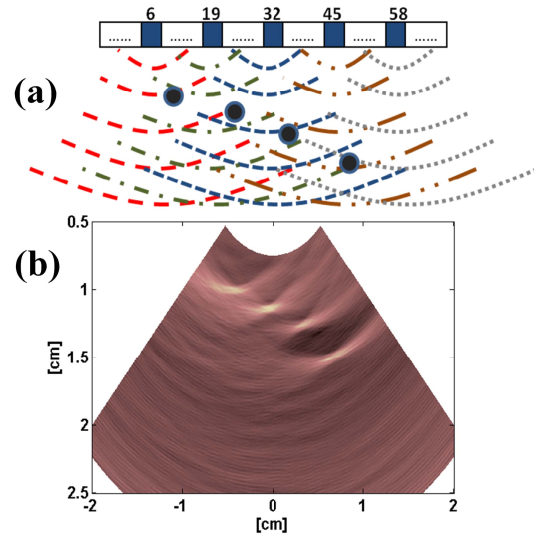


Fig. 9. (a) Schematic of the mismatched transmission CEs from five elements that insonify the field. All other elements were employed in the receive mode. (b) Final image generated by putting together five low-resolution images generated by transmission of FM1 to FM5 (experiment). This image was generated from simultaneous transmission of five 2-ms sinusoidal chirps with the very low amplitude of 20 mV$_{pp}$. DR is 22.3 dB and lateral resolution is 4.6 mm.

which was also used as the master board. The analog FGs and the data acquisition card were initiated by the output external trigger of the master FG board (PXI-5442). No power amplifier was used to boost the transmission signals. The schematic of the experiment with the abovementioned setup and mismatched transmission CEs from five elements is shown in Fig. 9(a). The sample was four 0.037 (0.92 mm) musical instrument wires (Malin Company, Cleveland, OH, USA) with approximately 3-mm in-between distance. The wires were held in a water tank in front of the transducer array.

As mentioned before, it turned out that the main challenge is the large crosstalk between the transmitting elements and adjacent receiving elements, which saturates the signal acquisition channels. To prevent this, 2-ms-long codes of a very low amplitude signal of 20 mV$_{pp}$ were used in the transmission. The five employed mismatched codes were sinusoidal chirps with a frequency range of 1 to 5 MHz and sweep patterns similar to FM1 to FM5 were introduced in Section II-A [Fig. 1(a)]. The detected signals from 59 elements of the array were used to calculate the CC signals with these five CEs and, therefore, to generate five low-resolution images corresponding to each transmitting element and code. Combining these images, the final image was produced and is shown in Fig. 9(b). It should be added that unlike normal pulsed or CE US, increasing signal averaging may not increase the image quality with this method, as it was shown that a small CC exists between different codes. These CCs represent artifacts in the image and increasing the number of averages intensifies them. However, increasing the duration of the code helps reduce such artifacts.

The employed signal duration of 2 ms is not normal in US applications. The presented example shows the feasibility of using long CEs without generating a large dead zone in the detection. It should be added that the employed frequency range is not optimal for SNR. Here the optimal BW is

TABLE II
SEQUENCE OF TEN FM SIGNALS TRANSMITTED EVERY 150 $\mu$s FROM FOUR ELEMENTS SIMULTANEOUSLY

| Transmitted Element | Sequential order of CEs transmitted every 150 μs | | | | | | | | | |
|---|---|---|---|---|---|---|---|---|---|---|
| #1 | FM1 | FM2 | FM3 | FM7* | FM4 | FM3 | FM2 | FM1 | FM4 | FM7 |
| #2 | FM3 | FM3* | FM1 | FM2 | FM3 | FM2 | FM4 | FM7 | FM2* | FM1 |
| #3 | FM4 | FM1 | FM4 | FM3 | FM1 | FM7* | FM1 | FM3 | FM3* | FM2 |
| #4 | FM2 | FM4 | FM7 | FM4* | FM7 | FM1 | FM3 | FM2 | FM1 | FM3 |

‘*’ indicates phase shift by 180°.

compromised to help reduce the CC among signals. The inverse relation between the BW and CC is shown in (4). It should be mentioned that the main challenge here is not SNR, and thus, even nonoptimal BW could generate a proper image. Although the presented schemes with five simultaneous transmissions can generate a high frame rate, they limit the penetration depth and lateral resolution and may cause artifacts due to the fixed location of transmissions. In addition, some of the elements are not acting in the receive mode, which not only reduces the number of receiving elements but also changes the required phase array pitch in those locations. The scheme that is presented next will resolve these issues.

### *B. Feasibility Test With Eight Transmitting Elements and Short Codes*

The number of transmitting elements plays a crucial role in the SNR of the signal [4]. To be able to use all elements of the transducer in the receive mode and also increase the number of transmitting elements, four extra multiplexer modules (NI PXI-2593) were employed. These multiplexers can switch between the transmitting and receiving elements and enable the use of all the elements in receive mode.

Furthermore, it was mentioned before that crosstalk among the elements of an array is a prevalent problem particularly for CE imaging dealing with long codes. In order to overcome the problem of crosstalk among the elements, the duration time of the CEs was reduced to as short as 12 $\mu$s. As a result, when the elements were receiving the signal from normal focal depths, the simultaneous transmissions did not interfere. By short codes, we mean that the code length is shorter than the depth of the field. Only four FGs were employed in this section. Since the crosstalk was circumvented, the maximum amplitude of the waveform generators, 10 $V_{pp}$, could be used in the transmitted signals. For the planned experiments and the focal distance of the array, the signal acquisition process does not require more than 150 $\mu$s to receive the response from the farthest objects. This short interval between transmissions enables a very high speed signal acquisition (6.667 kHz) and therefore facilitates performing averaging over the responses (as discussed in Section III). For instance, when the transmitted signal from one element is fixed, the phase or the starting time or the waveform of an adjacent transmitted signal can vary. As a consequence, the CC between each pair of the transmitted signals diminishes with averaging.

Two sets of waveforms were considered in the experiments: 1) a set of mismatched chirps and 2) a set of combined GC–FM. The mismatched chirps were generated using the sweep patterns shown in Fig. 1: FM1 to FM4 and FM7 with an identical duration of 12 $\mu$s. In addition, all the FMs share the same frequency range of 1.6–4.3 MHz. To perform effective averaging that diminishes the artifacts, each element transmitted ten successive CEs every 150 $\mu$s. The sequences of FM signals for four simultaneous transmitting elements are described in Table II. The location of transmitting elements was then permuted in four groups as depicted in Fig. 10. The eight elements used in transmission mode were 0, 9, 18, 27, 36, 45, 54, and 63. These elements were switched between the transmit and receive modes in four different groups. Using five different FMs provided a large number of possible permutations. Thus, the adjacent waveforms varied in each transmission (technique 4, Section III). The $*$ sign in Table II indicates that the phase of the CE was changed by 180° (technique 1, Section III).

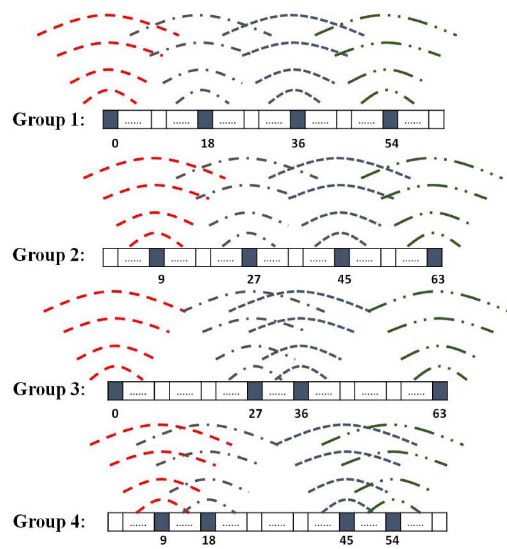


Fig. 10. Waveform transmission scheme in four groups. The transmitting elements are indicated with filled squares.

The abovementioned scheme was used to generate a US cross-sectional image of eight wires. Four simultaneous elements were used to transmit CE signals. One set of detected signals was collected as a result of these simultaneous transmissions. The pulse compressions were performed with the corresponding transmitted signals and they yielded four low-resolution images. Afterward, the transmitting elements

TABLE III

SEQUENCES OF FIVE COMBINED GC–FM SIGNALS TRANSMITTED EVERY 150 $\mu$S FROM FOUR ELEMENTS SIMULTANEOUSLY. ALSO SHOWN ARE THE COMPLEMENTARY GCs TRANSMITTED AFTER THE FIRST PARTS (SECOND PARTS)

| Transmitted Element | Sequential order of CEs transmitted every 150 μs: The first part of complementary GCs | | | | | The second part of complementary GCs | | | | |
|---|---|---|---|---|---|---|---|---|---|---|
| #1 | CGC1 | CGC2 | CGC4 | CGC10$^r$ | CGC4 | *CGC1* | *CGC2* | *CGC4* | *CGC10*$^r$ | *CGC4* |
| #2 | CGC10$^r$ | CGC1 | CGC2$^r$ | CGC4 | CGC2$^r$ | *CGC10*$^r$ | *CGC1* | *CGC2*$^r$ | *CGC4* | *CGC2*$^r$ |
| #3 | CGC2 | CGC4 | CGC10$^r$ | CGC1 | CGC1* | *CGC2* | *CGC4* | *CGC10*$^r$ | *CGC1* | *CGC1** |
| #4 | CGC4 | CGC10$^r$ | CGC1 | CGC2$^r$ | CGC10$^r$ | *CGC4* | *CGC10*$^r$ | *CGC1* | *CGC2*$^r$ | *CGC10*$^r$ |

'r' indicates employing reverse chirp.
'*' indicates phase shift by 180°.

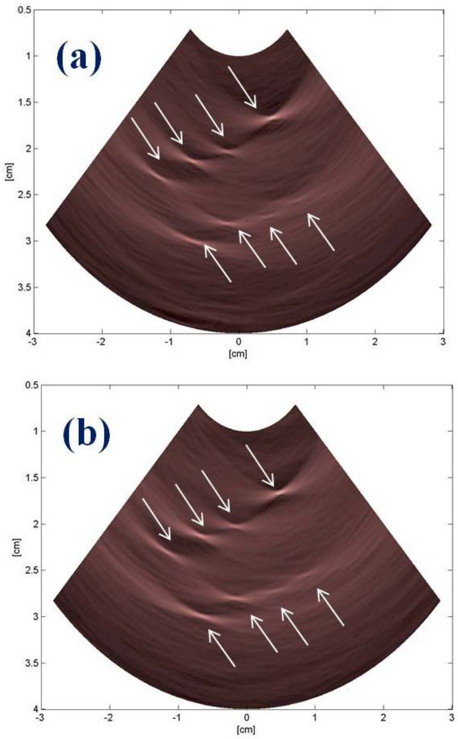


Fig. 11. US images of eight wires generated with (a) FM sequences described in Table II. (b) Combined GC–FM sequences described in Table III. The movies show the 16 low-resolution images generated in four simultaneous transmissions and four permutations of the elements and the final combined images. The arrows show the locations of the wires (experiment). DRs are 26.5 and 24.7 dB for (a) and (b), respectively. Lateral resolutions are 1.3 and 1.2 mm for (a) and (b), respectively.

were changed, and a new set of received signals was collected. This process was repeated for the four implemented groups (Fig. 10). Thus, 16 low-resolution images were produced. Superposition of the 16 images resulted in one final high-resolution image, shown in Fig. 11(a). The linked movie shows the 16 low-resolution images that yielded the final image.

In another experiment, the application of combined GC–FM signals for simultaneous multiple transmissions was investigated. Four different GCs with 1-, 2-, 4-, and 10-bit lengths were used to generate combined codes (Table I). The combined GC–FMs generated with the above mentioned GCs were labeled CGC1, CGC2, CGC4, and, CGC10, respectively. The sequences for four simultaneous transmissions are shown in Table III. CGC1 and CGC4 are the CEs shown in Fig. 3(b) and (c), respectively. CGC2 and CGC10 were also generated similarly by combining 2- and 10-bit GCs with upchirping FM. It is possible to use any other FM to generate more mismatched waveforms, for instance, downchirp FM2. The reverse sweep FM2 had also been used for some of the CEs that were marked with $r$ superscript in Table III. In addition, out-of-phase signals were marked with a $*$ sign as before, and here they are only used for CGC1. In the experiment, the sequence of five consecutive composite GCs was launched first, followed by the respective complementary codes as shown in Table III. The sequential insonifications were performed every 150 $\mu$s. As in the previous case, each group generated four simultaneous transmissions. The collected response signals were divided into two parts corresponding to the response to two complementary GCs. Similar to conventional GCs, each part was matched filtered and then both parts were added together to produce the final signal. Each set of collected data generated four sets of pulse compression signals corresponding to the transmitting elements. These signals were used to produce four low-resolution images and a total of 16 images for all groups. The final high-resolution image was generated through direct superposition of the 16 low-resolution images and is shown in Fig. 11(b). The linked movie shows the 16 low-resolution images and the final image. Both CEs were able to produce high-resolution images of approximately similar quality. The dynamic range (DR) of the FM scheme is somewhat higher than the combined GC–FM scheme, 26.5 dB versus 24.7 dB. The DRs of both Fig. 11(a) and (b) are higher than Fig. 9 (DR: 22.3 dB). Moreover, the lateral resolutions of Fig. 11(a) and (b) are 1.3 and 1.2 mm, which are significantly higher than the lateral resolution of 4.6 mm in Fig. 9. The use of eight transmitting elements versus five and the superposition of 16 low-resolution images versus 5 are the main reasons for the major quality enhancement of these images. The frame rate and the number of low-frequency images can be compared with a classical synthetic aperture method using the same hardware system. Eight elements were used as transmitters. Therefore, the classical individual transmission method required eight transmissions that provided eight low-frequency images. Here, we employed four transmissions (each consisting of four simultaneous signals) and generated 16 low-resolution images. The result increases the frame rate twofold along with the image quality. The duration times of transmission and acquisition signals allowed the frame rate to be as high as 167 Hz. This frame rate is only based on acquisition time and did not account for the processing of the data.

We conclude that combining the GC and FM can produce another source of mismatched CEs. It should be added that the combined GC–FM signals were produced with upchirp and downchirp sequences. Therefore, essentially only FM1 and FM2 with different GCs were used. There is no limitation in combining other chirp signals, such as FM3, FM4, and so on, with GCs. For instance, we can use a 4-b GC and combine that with different FM signals such as FM2 and FM3, thus generating multiple new mismatched codes. This arsenal of mismatched CEs is crucial for applications such as 3-D US imaging and transducers with thousands of elements.

## VI. CONCLUSION

Mismatched codes are signals with a very strong AC and a very weak CC among them. Two new methods for generating mismatched or weakly correlated CEs were presented in this paper. These methods can generate an unlimited number of FM chirps and combined GC–FMs that would enable simultaneous multiple-transmission US imaging. The combined GC–FM uses chirps as carrier waveforms for GCs and therefore produces a new family of codes. It was shown that as long as the slopes of the FM signals in different combinations of GC–FM signals are different, they have a weak CC.

The minimal CC among these codes facilitates temporal encoding of the field insonification, and therefore, the response of each CE can be handled independently. An important advantage of the presented mismatched codes is that they have an identical BW and CF. Therefore, their use will not compromise SNR or resolution. In addition, the new techniques do not use Hadamard encoding, so they can enhance the frame rate much more than methods that do use this encoding. Another advantage of the presented methods is that the mismatched codes can be readily generated in a computer algorithm, which facilitates applications for transducer arrays with a large number of elements.

The feasibility of the method was experimentally demonstrated on very simple musical instrument wire samples. Very long CEs were tried to take advantage of SNR enhancement of CE and at the same time reduce the CC between the codes. The main challenge of using long codes, however, was the large crosstalk between the elements of the transducer array. Increasing the number of averages in this case was not helpful as it enhanced the CC between the mismatched codes and, thus, the artifacts. Increasing the signal duration and reducing the transmission power was found to be a solution for both crosstalk and artifacts. More practical methods for overcoming these problems were also discussed. In another set of experiments, the use of short codes was examined. In these experiments, different permutations of codes and transmission elements enabled the reduction of artifacts due to weak CC between the codes.

All these new mismatched codes can be employed together to facilitate multiple transmissions from a large number of elements and generate 3-D US images. It should be emphasized that the presented methods are not only useful for biomedical US imaging, but also there is a definite need in many similar fields such as sonar [17], radar [18], NDE US, as well as photoacoustics (PA). The mismatched chirps have already been employed in PA for simultaneous *in vivo* functional imaging with two wavelengths [34].

## APPENDIX
## CROSS CORRELATION OF TWO LINEAR FREQUENCY MODULATION CHIRPS WITH IDENTICAL BANDWIDTH AND DIFFERENT FREQUENCY SWEEP SLOPES

An LFM can be described as

$$r_1(t) = \cos\left(\omega_c t + \frac{\pi\mu_1}{2}t^2\right)\mathrm{rect}\left(\frac{t}{T_{\mathrm{LFM1}}}\right) \tag{A-1}$$

where $\mu_1 = (\Delta\omega/T_{\mathrm{LFM1}}) = (2\pi B_{\mathrm{FM}}/T_{\mathrm{LFM1}})$ is the slope and $T_{\mathrm{LFM1}}$, $B_{\mathrm{FM}}$, and $\omega_c$ are the chirp duration, the frequency BW, and the central angular frequency of the chirp, respectively. The AC of $r_1(t)$ in (A-1) for large time–BW product has been calculated [25]

$$\begin{aligned} R_{11}(t) &= r_1(t) * r_1(-t) \\ &\approx \frac{\sin(\mu_1 T_{\mathrm{FM1}} t/2)}{\mu_1 t}\cos(\omega_c t)\mathrm{rect}\left(\frac{t}{2T_{\mathrm{FM1}}}\right) \end{aligned} \tag{A-2}$$

with peak value $R_{11\,\max} \approx (T_{\mathrm{FM1}}/2)$. The Fourier transform of (A-1) is shown to be [25]

$$\begin{aligned} S_1(\omega) = |S_1(\omega)| \exp\left[-j\frac{(\omega-\omega_c)^2}{2\mu_1}\right] \\ \times \exp\left[j\tan^{-1}\frac{S(X_1)+S(X_2)}{C(X_1)+C(X_2)}\right]. \end{aligned} \tag{A-3}$$

The three terms are amplitude, square-law phase, and residual phase terms, respectively. The amplitude term is

$$|S_1(\omega)| = \frac{1}{2}\sqrt{\frac{\pi}{\mu_1}}\{[C(X_1)+C(X_2)]^2 + [S(X_1)+S(X_2)]^2\}^{\frac{1}{2}} \tag{A-4}$$

where $C()$ and $S()$ are Fresnel integrals and $X_1$ and $X_2$ are

$$X_{1,2} = \frac{\frac{\mu_1 T_{\mathrm{FM1}}}{2} \pm (\omega-\omega_c)}{\sqrt{\pi\mu_1}}.$$

For large time–BW products, the residual phase term can be ignored (a constant phase) and the combination of the Fresnel integral terms is normally approximated with their value at $\omega = \omega_c$, that is, $\sqrt{2}$ [2], [25]. Therefore, in the corresponding BW range of $\omega_1 - \omega_2$, we obtain $(\Delta\omega = \omega_2 - \omega_1)$

$$S_1(\omega) \approx \sqrt{\frac{\pi}{2\mu_1}}\exp\left[-j\frac{(\omega-\omega_c)^2}{2\mu_1}\right]\mathrm{rect}\left(\frac{|\omega|-\omega_c}{\Delta\omega}\right). \tag{A-5}$$

By matched filtering in frequency domain, the phase terms in $S_1(\omega)$ and $S_1^*(\omega)$ cancel each other out and yield

$$\begin{aligned} R_{11}(t) &= F^{-1}\{S_1(\omega)S_1^*(\omega)\} \approx F^{-1}\left\{\frac{\pi}{2\mu_1}\mathrm{rect}\left(\frac{|\omega|-\omega_c}{\Delta\omega}\right)\right\} \\ &= \frac{\Delta\omega}{2\mu_1}\sin c(\Delta\omega t)\cos(\omega_c t). \end{aligned} \tag{A-6}$$

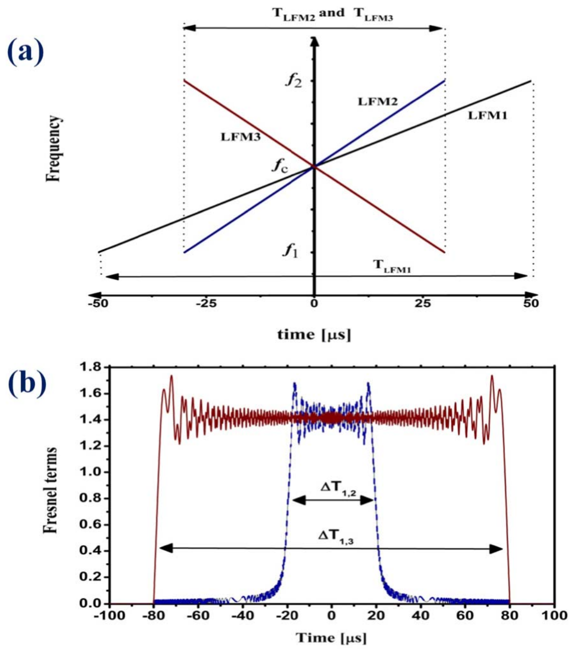


Fig. 12. (a) Three linear frequency sweeps with identical frequency ranges and different slopes. (b) CC of LFM2 and LFM3 with LFM1 described in (a) normalized by the factor $(1/\sqrt{2})(T_{\mathrm{LFM1}}T_{\mathrm{LFM2\ or\ 3}}/B_{\mathrm{FM}}\Delta T)^{1/2}\sqrt{2}$. Therefore, the plots correspond to the Fresnel term in (A-12). In (A-12), the Fresnel term is approximated with its value at $t = 0$, that is, $\sqrt{2}$. Here, the frequency range is 1–4 MHz, and $T_{\mathrm{LFM1}} = 100\ \mu$s and $T_{\mathrm{LFM2}} = T_{\mathrm{LFM3}} = 60\ \mu$s.

This is identical to (A-2). Now, we can consider another LFM chirp with a different slope, for instance, $\mu_2$ [Fig. 12(a)]

$$r_2(t) = \cos\left(\omega_c t + \frac{\pi\mu_2}{2}t^2\right)\mathrm{rect}\left(\frac{t}{T_{\mathrm{LFM2}}}\right). \tag{A-7}$$

Similarly, the Fourier transform of this LFM can be approximated as

$$S_2(\omega) \approx \sqrt{\frac{\pi}{2\mu_2}}\exp\left[-j\frac{(\omega-\omega_c)^2}{2\mu_2}\right]\mathrm{rect}\left(\frac{|\omega|-\omega_c}{\Delta\omega}\right). \tag{A-8}$$

Using the approximate value of the Fresnel terms (the value at $\omega = \omega_c$), the mismatched CC of $r_1$ and $r_2$ can be estimated

$$\begin{aligned} R_{12}(t) &= F^{-1}\{S_2(\omega)S_1^*(\omega)\} \\ &\approx F^{-1}\left\{\frac{\pi}{2\sqrt{|\mu_1\mu_2|}}\exp\left[-j\frac{(\omega-\omega_c)^2}{2}\left(\frac{1}{\mu_2}-\frac{1}{\mu_1}\right)\right]\right. \\ &\qquad \left.\times\ \mathrm{rect}\left(\frac{|\omega|-\omega_c}{\Delta\omega}\right)\right\}. \end{aligned} \tag{A-9}$$

It should be noted that although the slopes share the same BW, they can have different directions, i.e., upchirp or downchirp. We define two new parameters, $\Delta T$ and $\mu_{\mathrm{eq}}$

$$\begin{aligned} \mu_{\mathrm{eq}} &\equiv \frac{\mu_2\mu_1}{\mu_1-\mu_2} \\ \Delta T &\equiv |\mathrm{sign}(\mu_1)T_{\mathrm{LFM2}} - \mathrm{sign}(\mu_2)T_{\mathrm{LFM1}}| \end{aligned} \tag{A-10}$$

and thus

$$|\mu_1-\mu_2| = \frac{2\pi B_{\mathrm{FM}}}{T_{\mathrm{LFM1}}T_{\mathrm{LFM2}}}\Delta T. \tag{A-11}$$

Therefore

$$\begin{aligned} R_{12}(t) &\approx F^{-1}\left\{\frac{\pi}{2\sqrt{\mu_1\mu_2}}\exp\left[-j\frac{(\omega-\omega_c)^2}{2\mu_{\mathrm{eq}}}\right]\mathrm{rect}\left(\frac{|\omega|-\omega_c}{\Delta\omega}\right)\right\} \\ &= \frac{\pi}{2\sqrt{\mu_1\mu_2}}\sqrt{\frac{2\mu_{\mathrm{eq}}}{\pi}}e^{j\left(\omega_c t+\frac{\mu_{\mathrm{eq}}}{2}t^2+\theta_2(t)\right)} \\ &= \sqrt{\frac{\pi}{2|\mu_1-\mu_2|}}e^{j\left(\omega_c t+\frac{\mu_{\mathrm{eq}}}{2}t^2+\theta_2(t)\right)} \\ &= \sqrt{\frac{T_{\mathrm{LFM1}}T_{\mathrm{LFM2}}}{4B_{\mathrm{FM}}\Delta T}}e^{j\left(\omega_c t+\frac{\mu_{\mathrm{eq}}}{2}t^2+\theta_2(t)\right)}. \end{aligned} \tag{A-12}$$

The above term was calculated by substituting the Fresnel term with its value at $t = 0$ (that is, $\sqrt{2}$). Since we are looking for the maximum value, this approximation is not proper, but the maximum of Fresnel ripples should be replaced approximately by $1.2\sqrt{2}$ [Fig. 12(b)]. Therefore, the maximum amplitude of the CC between two LFM chirps with different slopes and an identical BW is approximately $(1.2/2)(T_{\mathrm{LFM1}}T_{\mathrm{LFM2}}/B_{\mathrm{FM}}\Delta T)^{1/2}$. It should be noted that in the presented formula, the substitution (exchanging of) $r_1$ and $r_2$ does not change the CC between them

$$\begin{aligned} \mathrm{CC}_{12}|_{\max} = \mathrm{CC}_{21}|_{\max} &\approx \frac{1.2}{2}\sqrt{\frac{T_{\mathrm{LFM1}}T_{\mathrm{LFM2}}}{B_{\mathrm{FM}}\Delta T}} \\ &= 1.2\sqrt{\frac{\pi}{2|\mu_1-\mu_2|}} \end{aligned}$$

where

$$\Delta T = |\mathrm{sign}(\mu_1)T_{\mathrm{LFM2}} - \mathrm{sign}(\mu_2)T_{\mathrm{LFM1}}|. \tag{A-13}$$

However, the CC/AC depends on the AC of $r_1$ or $r_2$

$$\frac{\mathrm{CC}_{1,2}}{\mathrm{AC}_1} \approx \frac{\frac{1.2}{2}\sqrt{\frac{T_{\mathrm{LFM1}}T_{\mathrm{LFM2}}}{B_{\mathrm{FM}}\Delta T}}}{\frac{T_{\mathrm{LFM1}}}{2}} = 1.2\sqrt{\frac{T_{\mathrm{LFM2}}}{T_{\mathrm{LFM1}}B_{\mathrm{FM}}\Delta T}} \tag{A-14}$$

$$\frac{\mathrm{CC}_{1,2}}{\mathrm{AC}_2} \approx \frac{\frac{1.2}{2}\sqrt{\frac{T_{\mathrm{LFM1}}T_{\mathrm{LFM2}}}{B_{\mathrm{FM}}\Delta T}}}{\frac{T_{\mathrm{LFM2}}}{2}} = 1.2\sqrt{\frac{T_{\mathrm{LFM1}}}{T_{\mathrm{LFM2}}B_{\mathrm{FM}}\Delta T}}. \tag{A-15}$$

This result is consistent with the calculations shown in [2] and [25] in the sense that CC/AC of two LFMs is proportional to $1/\sqrt{B_{\mathrm{FM}}\Delta T}$. However, as shown here, the CC/AC also depends on the duration of both LFMs. Therefore, to reduce the CC/AC, one can increase the BW or $\Delta T$.

## References

[1] M. O'Donnell, "Coded excitation system for improving the penetration of real-time phased-array imaging systems," *IEEE Trans. Ultrason., Ferroelectr., Freq. Control*, vol. 39, no. 3, pp. 341–351, May 1992.

[2] T. Misaridis and J. A. Jensen, "Use of modulated excitation signals in medical ultrasound. Part III: High frame rate imaging," *IEEE Trans. Ultrason., Ferroelectr., Freq. Control*, vol. 52, no. 2, pp. 208–219, Feb. 2005.

[3] M. Karaman, P.-C. Li, and M. O'Donnell, "Synthetic aperture imaging for small scale systems," *IEEE Trans. Ultrason., Ferroelectr., Freq. Control*, vol. 42, no. 3, pp. 429–442, May 1995.

[4] J. A. Johnson, M. Karaman, and B. T. Khuri-Yakub, "Coherent-array imaging using phased subarrays. Part I: Basic principles," *IEEE Trans. Ultrason., Ferroelectr., Freq. Control*, vol. 52, no. 1, pp. 37–50, Jan. 2005.

[5] J. A. Jensen, S. I. Nikolov, K. L. Gammelmark, and M. H. Pedersen, "Synthetic aperture ultrasound imaging," *Ultrasonics*, vol. 44, pp. e5–e15, Dec. 2006.

[6] I. Trots, Y. Tasinkevych, A. Nowicki, and M. Lewandowski, "Golay coded sequences in synthetic aperture imaging systems," *Arch. Acoust.*, vol. 36, no. 4, pp. 913–926, 2011, doi: 10.2478/v10168-011-0061-5.

[7] M. O'Donnell and Y. Wang, "Coded excitation for synthetic aperture ultrasound imaging," *IEEE Trans. Ultrason., Ferroelectr., Freq. Control*, vol. 52, no. 2, pp. 171–176, Feb. 2005.

[8] R. Y. Chiao and L. J. Thomas, "Method and apparatus for ultrasonic synthetic transmit aperture imaging using orthogonal complementary codes," U.S. Patent 6 048 315, Apr. 11, 2000.

[9] R. Y. Chiao and L. J. Thomas, "Synthetic transmit aperture imaging using orthogonal Golay coded excitation," in *Proc. IEEE Ultrason. Symp.*, Oct. 2000, pp. 1677–1680.

[10] J. Shen and E. S. Ebbini, "A new coded-excitation ultrasound imaging system. I. Basic principles," *IEEE Trans. Ultrason., Ferroelectr., Freq. Control*, vol. 43, no. 1, pp. 131–140, Jan. 1996.

[11] M. K. Kiymik, I. Güler, O. Hasekioglu, and M. Karaman, "Ultrasound imaging based on multiple beamforming with coded excitation," *Signal Process.*, vol. 58, no. 1, pp. 107–113, Apr. 1997.

[12] P. Gong, M. C. Kolios, and Y. Xu, "Delay-encoded transmission and image reconstruction method in synthetic transmit aperture imaging," *IEEE Trans. Ultrason., Ferroelectr., Freq. Control*, vol. 62, no. 10, pp. 1745–1756, Oct. 2015.

[13] F. Gran and J. A. Jensen, "Multi element synthetic aperture transmission using a frequency division approach," in *Proc. IEEE Ultrason. Symp.*, Oct. 2003, pp. 1942–1946.

[14] F. Gran and J. A. Jensen, "Spatio-temporal encoding using narrow-band linear frequency modulated signals in synthetic aperture ultrasound imaging," *Proc. SPIE*, vol. 5750, pp. 405–416, Apr. 2005.

[15] B.-H. Kim and T.-K. Song, "Multibeam simultaneous transmit multi-zone (MB-STMZ) focusing method using modulated orthogonal codes for ultrasound imaging," *Proc. SPIE*, vol. 5373, pp. 315–323, Apr. 2004.

[16] J. S. Hwang and T. K. Song, "Ultrasound imaging apparatus and method using Golay codes with orthogonal property," U.S. Patent 6 547 733 B2, Apr. 15, 2003.

[17] J. S. Jaffe and P. M. Cassereau, "Multibeam imaging using spatially variant insonification," *J. Acoust. Soc. Amer.*, vol. 83, no. 4, pp. 1458–1464, 1988.

[18] T. Sakamoto and T. Sato, "Code-division multiple transmission for high-speed UWB radar imaging with an antenna array," *IEEE Trans. Geosci. Remote Sens.*, vol. 47, no. 4, pp. 1179–1186, Apr. 2009.

[19] S. D. Silverstein, "Application of orthogonal codes to the calibration of active phased array antennas for communication satellites," *IEEE Trans. Signal Process.*, vol. 45, no. 1, pp. 206–218, Jan. 1997.

[20] D. S. Purdy and A. Jacomb-Hood, "In orbit active array calibration for NASA's LightSAR," in *Proc. IEEE Radar Conf.*, Apr. 1999, pp. 172–176.

[21] T. Misaridis and J. A. Jensen, "Use of modulated excitation signals in medical ultrasound. Part II: Design and performance for medical imaging applications," *IEEE Trans. Ultrason., Ferroelectr., Freq. Control*, vol. 52, no. 2, pp. 192–207, Feb. 2005.

[22] M. Golay, "Complementary series," *IRE Trans. Inf. Theory*, vol. IT-7, no. 2, pp. 82–87, Apr. 1961.

[23] M. Pollakowski, H. Ermert, L. von Bernus, and T. Schmeidl, "The optimum bandwidth of chirp signals in ultrasonic applications," *Ultrasonics*, vol. 31, no. 6, pp. 417–420, Nov. 1993.

[24] B. Lashkari and A. Mandelis, "Linear frequency modulation photoacoustic radar: Optimal bandwidth and signal-to-noise ratio for frequency-domain imaging of turbid media," *J. Acoust. Soc. Amer.*, vol. 130, no. 3, pp. 1313–1324, 2011.

[25] C. E. Cook and M. Bernfeld, *Radar Signals: An Introduction to Theory and Application*. New York, NY, USA: Academic, 1967.

[26] B. Lashkari and A. Mandelis, "Photoacoustic radar imaging signal-to-noise ratio, contrast, and resolution enhancement using nonlinear chirp modulation," *Opt. Lett.*, vol. 35, no. 10, pp. 1623–1625, 2010.

[27] M. Pollakowski and H. Ermert, "Chirp signal matching and signal power optimization in pulse-echo mode ultrasonic nondestructive testing," *IEEE Trans. Ultrason., Ferroelectr., Freq. Control*, vol. 41, no. 5, pp. 655–659, Sep. 1994.

[28] S. A. Telenkov, R. Alwi, and A. Mandelis, "Photoacoustic correlation signal-to-noise ratio enhancement by coherent averaging and optical waveform optimization," *Rev. Sci. Instrum.*, vol. 84, no. 10, p. 104907, 2013.

[29] A. Nowicki, I. Trots, P. A. Lewin, W. Secomski, and R. Tymkiewicz, "Influence of the ultrasound transducer bandwidth on selection of the complementary Golay bit code length," *Ultrasonics*, vol. 47, nos. 1–4, pp. 64–73, Dec. 2007.

[30] B. Lashkari, A. Manbachi, A. Mandelis, and R. S. C. Cobbold, "Slow and fast ultrasonic wave detection improvement in human trabecular bones using Golay code modulation," *J. Acoust. Soc. Amer.*, vol. 132, no. 3, pp. EL222–EL228, 2012.

[31] R. S. C. Cobbold, *Foundations of Biomedical Ultrasound*. London, U.K.: Oxford Univ. Press, 2007.

[32] G. Montaldo, M. Tanter, J. Bercoff, N. Benech, and M. Fink, "Coherent plane-wave compounding for very high frame rate ultrasonography and transient elastography," *IEEE Trans. Ultrason., Ferroelectr., Freq. Control*, vol. 56, no. 3, pp. 489–506, Mar. 2009.

[33] S. Telenkov, R. Alwi, A. Mandelis, and A. Worthington, "Frequency-domain photoacoustic phased array probe for biomedical imaging applications," *Opt. Lett.*, vol. 36, no. 23, pp. 4560–4562, 2011.

[34] B. Lashkari, S. S. S. Choi, M. E. Khosroshahi, E. Dovlo, and A. Mandelis, "Simultaneous dual-wavelength photoacoustic radar imaging using waveform engineering with mismatched frequency modulated excitation," *Opt. Lett.*, vol. 40, no. 7, pp. 1145–1148, 2015.


**Bahman Lashkari** received the Ph.D. degree in frequency-domain photoacoustic imaging from the Centre for Advanced Diffusion-Wave Technologies (CADIFT), Toronto, ON, Canada, in 2011, with a focus on frequency-domain photoacoustic imaging.

He is currently a Postdoctoral Research Associate with CADIFT, University of Toronto, Toronto, where he is involved in several photoacoustic and ultrasound projects. His current research interests include medical imaging and tissue characterization.

**Kaicheng Zhang** is an undergraduate student in mechanical engineering from the University of Toronto, Toronto, ON, Canada. He is currently pursuing academic advancement in medical equipment development.

His current research interests include discovering novel techniques and applications in ultrasonic and photoacoustic imaging.

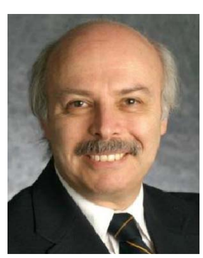

**Andreas Mandelis** is currently a Full Professor of Mechanical and Industrial Engineering, and Electrical and Computer Engineering with the Institute of Biomaterials and Biomedical Engineering, University of Toronto, Toronto, ON, Canada. He is the Director of the Center for Advanced Diffusion-Wave Technologies, Toronto. He has authored or coauthored over 360 scientific papers in refereed journals and 180 scientific and technical proceedings papers.

Prof. Mandelis is the Editor-in-Chief of the *International Journal of Thermophysics* and an Editor of the *Journal of Biomedical Optics*, the *Journal of Applied Physics*, and *Optics Letters*.